JACS
JOURNAL OF THE AMERICAN CHEMICAL SOCIETY

Article

pubs.acs.org/JACS

One-Dimensional Fluorescent Silicon Nanorods Featuring Ultrahigh Photostability, Favorable Biocompatibility, and Excitation Wavelength-Dependent Emission Spectra

Bin Song, Yiling Zhong, Sicong Wu, Binbin Chu, Yuanyuan Su, and Yao He*

Jiangsu Key Laboratory for Carbon-Based Functional Materials and Devices, Institute of Functional Nano & Soft Materials (FUNSOM), and Collaborative Innovation Center of Suzhou Nano Science and Technology (NANO−CIC), Soochow University, Suzhou, Jiangsu 215123, China

Supporting Information

ABSTRACT: We herein report a kind of one-dimensional biocompatible fluorescent silicon nanorods (SiNRs) with tunable lengths ranging ∼100−250 nm, which can be facilely prepared through one-pot microwave synthesis. In addition to the strong fluorescence (quantum yield value: ∼15%) and negligible toxicity, the resultant SiNRs exhibit excitation wavelength-dependent photoluminescence whose maximum emission wavelength ranges from ∼450 to ∼600 nm under serial excitation wavelengths from 390 to 560 nm, providing feasibility for multicolor biological imaging. More significantly, the SiNRs are ultrahighly photostable, preserving strong and nearly unchanged fluorescence under 400 min high-power UV irradiation, which is in sharp contrast to severe fluorescence quenching of organic dyes (e.g., FITC) or II−VI quantum dots (QDs) (e.g., CdTe QDs and CdSe/ZnS QDs) within 15 or 160 min UV treatment under the same experiment conditions, respectively. Taking advantage of these attractive merits, we further exploit the SiNRs as a novel type of color converters for the construction of white light-emitting diodes (LED), which is the first proof-of-concept demonstration of LED device fabricated using the one-dimensional fluorescent silicon nanostructures.

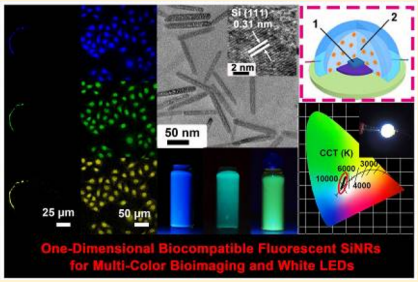

INTRODUCTION

Silicon materials are of great importance for both fundamental research and practical applications, which has dominated the semiconductor industry in the last century.[1] Accompanied with significant advancement of nanoscale fabrication techniques, one-dimensional functional silicon nanomaterials have been elegantly developed as new powerful tools for potentially promoting silicon-based semiconducting technology.[1e−i] Typically, in virtue of scientists' elegant work, silicon nanowires (SiNWs), which are recognized as representative one-dimensional silicon nanostructures, have been well developed and widely utilized for various applications, including field-effect transistor, surface-enhanced Raman scattering sensor, drug carrier, solar cell, nanomechanical device, lithium-ion battery, etc.[2−4] For example, taking advantage of superior electronic merits of SiNWs, Lieber et al. have developed a series of SiNWs-based sensors, suitable for specific and sensitive detection of biological species (e.g., DNA and cells).[2a,b] Very recently, they further explored a kind of metal oxide passivated SiNWs-based sensor, opening up new avenues for implantation and long-term brain activity mapping.[3] Yang and co-workers introduced a low-temperature wafer-scale etching and thin-film deposition method for fabricating silicon n-p core−shell nanowire solar cells.[4a] They further reported that the SiNWs harvest light energy to provide reducing equivalents to the anaerobic bacterium.[4b] Using the unique mechanical properties of silicon, the same group presented the first demonstration of a direct interface of SiNWs with mammalian cells without any external force.[4c]

On the other hand, one-dimensional fluorescent silicon nanostructures have been recently drawn intensive research interest because their unique optical properties can differ significantly from zero-dimensional silicon nanoparticles.[5] Specifically, radiative electron−hole recombination rates and Auger recombination existing in one-dimensional nanostructures could largely lower thresholds for optical gain and multiexciton generation, which are significant for higher-performance photovoltaic devices and nanolasers.[5b,c] However, bulk silicon exhibits poor emission and small near band gap absorption. It is worth pointing out that theoretical calculation reveals that nanoscale silicon can exhibit luminescence because the overlap of the electron and hole wave functions is distinctly increased, leading to dramatic enhancement of recombination rates of electrons and holes.[5d,e]

Recently, Korgel and co-workers experimentally presented the first example of one-dimensional fluorescent silicon nanostructures, i.e., silicon nanorods (SiNRs). In their study, the fluorescent SiNRs with quantum yields (QY) of 4−5% were prepared by the decomposition of trisilane (Si_3H_8) in hot squalane (at 410 °C) in the presence of dodecylamine and tin (Sn) nanocrystals, followed by HF-etching treatment and thermal hydrosilylation.[6] Notably, compared to the sufficient

Received: January 14, 2016
Published: March 24, 2016

DOI: 10.1021/jacs.6b00479
J. Am. Chem. Soc. 2016, 138, 4824−4831

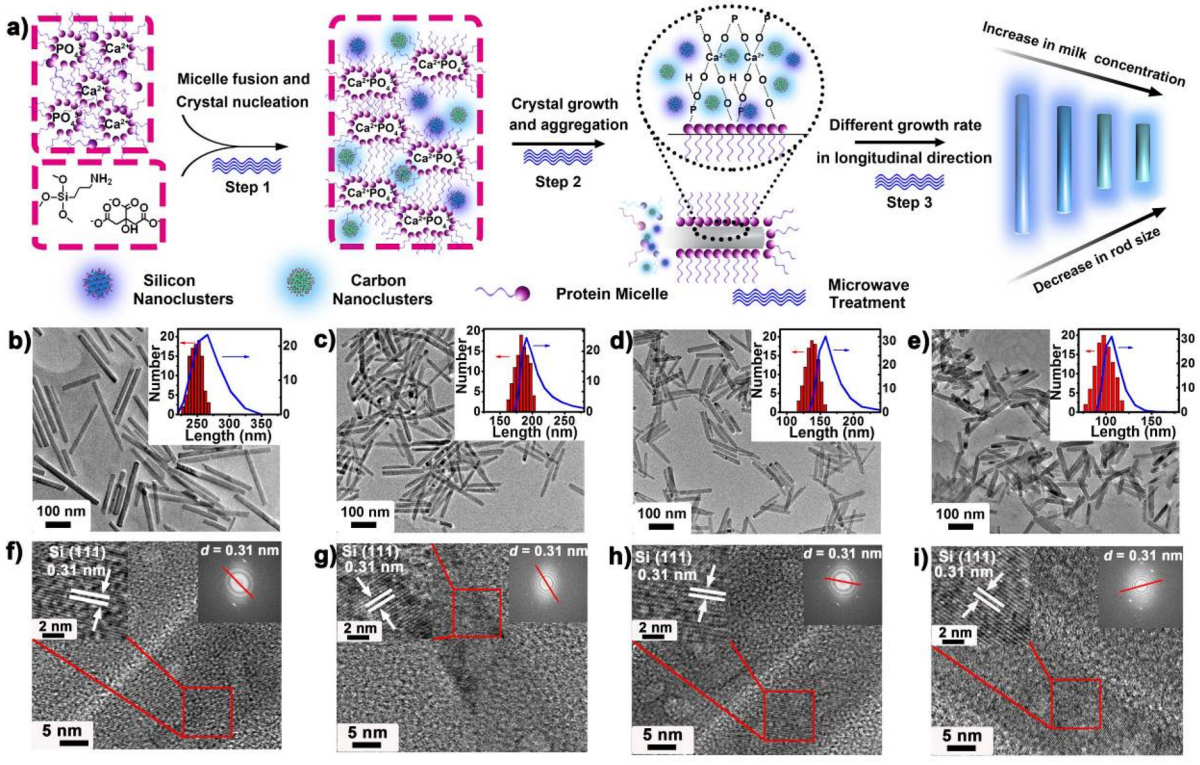

Figure 1. (a) Schematic illustration of microwave synthesis of SiNRs. The whole growth process is composed of three typical steps: micelle fusion and crystal nucleation (Step1), crystal growth and aggregation (Step 2), and different growth rate in longitudinal direction (Step 3). (b–i) TEM and HRTEM images of SiNRs with different lengths: (b, f) 250 nm; (c, g) 180 nm; (d, h) 140 nm; and (e, i) 100 nm at different milk concentrations ranging from 1 to 4 mg/mL. Insets in (b–e) represent corresponding length distribution analysis (histograms) determined by TEM and DLS spectra (blue curves).

progress of SiNWs-related investigations, this is merely one example of fluorescent SiNRs, which nevertheless involves relatively complicated long-term synthetic procedures, harsh experimental conditions (e.g., high temperature), and low QY values as mentioned above. Moreover, to the best of our knowledge, there currently exists no report concerning one-dimensional fluorescent silicon nanostructure-based optoelectronic devices, leading to difficulties in the exploration of one-dimensional fluorescent silicon nanostructures for widespread optical applications.

In this paper, we present a kind of highly fluorescent and photostable SiNR, which can be readily prepared through an one-pot microwave synthesis in aqueous phase under mild reaction conditions (e.g., reaction temperature/time: 150 °C/60 min). The obtained SiNRs exhibit bright fluorescence (quantum yield: ~15%), excellent storage and photostability (preserving ~90% of the initial intensity after 100 days of storage or 400 min UV irradiation), favorable biocompatibility (SiNRs-treated human epithelial cervical cancer (HeLa) cells maintained above 90% at serial concentrations (0.125–2 mg/mL), and incubation times (0.5–48 h) as well as continuous excitation-dependent emission spectra (maximum emission wavelengths range from ~450 to ~600 nm, corresponding to excitation wavelengths from 390 to 560 nm). Of particular note, taking advantage of these attractive merits, the first example of one-dimensional fluorescent silicon nanostructure-based white-light-emitting devices is constructed by using the resultant SiNRs as novel color converters.

RESULTS AND DISCUSSION

Microwave dielectric heating is attractive owing to its unique merits (e.g., rapid and homogeneous heating, excellent reaction selectivity, etc.), which has been widely utilized for the preparation of functional nanostructures (e.g., nanodots, nanorods, and nanowires), including our recent success in the development of microwave-assisted methods for synthesizing zero-dimensional fluorescent silicon nanoparticles (SiNPs).[7] Inspired by these previous studies, in this current work, microwave irradiation is exploited for the synthesis of one-dimensional fluorescent SiNRs with tunable lengths, as schematically illustrated in Figure 1a. In brief, the $C_6H_{17}NO_3Si$ molecules could be readily reduced by trisodium citrate, and the albumens from milk could be readily pyrolyzed through microwave irradiation, leading to the creation of silicon and carbon nanoclusters (Step 1). In addition, previous investigation has demonstrated that the majority of the protein (i.e., casein) in milk is readily incorporated into large colloidal structures known as protein micelles, which could be further linked together with colloidal calcium phosphate (CaP).[8] The micelles radii depend on the origin concentration of the milk.[8b] Following the addition of the silicon source, fusion–fission between the protein micelles induces the reaction between calcium (Ca) and phosphate (P) ions and finally the formation of CaP crystals under microwave irradiation.[9] Notably, the addition of aminosilane most likely facilitates the CaP formation by oriented attachment of the coupling agent to CaP crystals which is favorable for the creation of one dimension rod-structured nanomaterials.[9b] A similar mechanism was proposed previously for CaP crystallization in the

DOI: 10.1021/jacs.6b00479
J. Am. Chem. Soc. 2016, 138, 4824–4831

body with the support of certain proteins.[9c] Therefore, in our case, the formed CaP nucleation facilitates the aggregation of primary silicon and carbon nuclei, leading to the formation of an one-dimensional nanostructure under microwave irradiation, as shown in Step 2. On the other hand, according to the La Mer curve (recognized as one of the classical crystallization mechanisms),[10] nucleation and crystal growth rates in longitudinal direction are largely influenced by the supersaturation level of synthesis system. Specifically, the larger crystals are prone to be formed at a low supersaturation level in which crystals growth rate is much faster than nucleation rate, while the smaller crystals are easily formed at a high supersaturation level where crystal growth is slower than nucleation rate. As a result, a higher milk concentration that corresponds to higher supersaturation levels will result in faster nucleation and thus shorter SiNRs. Similarly, low milk concentration will lead to low supersaturation and the formation of longer nanorods, as shown in Step 3. As a control, $C_6H_{17}NO_3Si$ molecules or pure milk is respectively used as the reaction precursor alone, which can only produce SiNPs or carbon NPs instead (Figure S1).

Figure 1b–e shows typical transmission electronic microscope (TEM) images of SiNRs with tunable lengths, which are obtained at different milk concentrations varying from 1 to 4 mg/mL, while keeping other synthesis parameters constant. Fairly uniform nanorods are observed in all samples, and the length of rods clearly became shorter with increasing milk concentration. The size measurement based on TEM images also confirms a very narrow length distribution of the rods (insets in Figure 1b–e) and shows that the lengths of the SiNRs are ~100, ~140, ~180, and ~250 nm, which are similar to the results of ~105, ~165, ~190, and ~260 nm measured by dynamic light scattering (DLS), respectively (as indicated by the blue curves in insets of Figure 1b–e). The slight difference is due to different test environments between TEM and DLS characterization, as discussed in previous reports.[7e,f] As a result, the aspect ratios of these nanorods are systematically tuned from 12.5 to 4.9, simply by adjusting the milk concentrations from 1 to 4 mg/mL (12.5 (1 mg/mL), 9.2 (2 mg/mL), 6.9 (3 mg/mL), and 4.9 (4 mg/mL)). The relatively constant diameter indicates that the growth of all nanorods is mainly limited in the transverse direction. When the milk concentration increases to 4 mg/mL, the supersaturation reaches a high level; therefore, the length of nanorods without significant change is observed beyond this concentration. According to high-resolution TEM (HRTEM) images (Figure 1f–i), the prepared SiNRs with different length show well-defined lattice fringes, relative to (111) planes of cubic crystalline silicon (lattice spacing: 0.31 nm). Corresponding fast Fourier transform is also presented (Figure 1f–i inset), in which the set of spots with a lattice spacing of 0.31 nm can be indexed to the (111) reflection, providing convincing demonstration of high crystallinity of the resultant SiNRs.[11]

The resultant SiNRs are systematically characterized by X-ray powder diffraction (XRD), Fourier transform infrared spectroscopy (FTIR), Raman, X-ray photoelectron spectra (XPS), electron dispersive X-ray spectra (EDX), and thermal gravity analysis (Figures 2 and S3–S6). As shown in Figure 2, the XRD patterns of SiNRs with different aspect ratio consist of diffraction peaks derived from the cubic phase of silicon at 28.4° (111), 47.3° (220), and 56.1° (311) (JCPDF card no. 89-5012). As one type of CaP crystalline structures, hydroxyapatite is confirmed by XRD, where the diffraction peaks are consistent

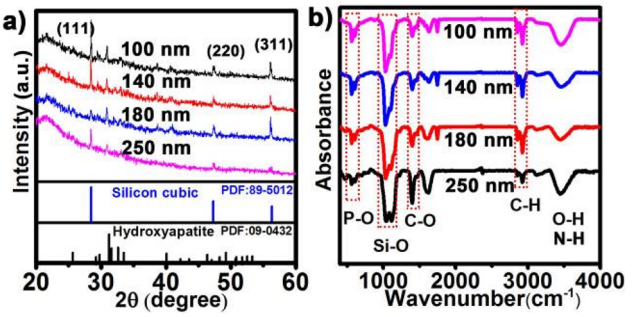

Figure 2. (a) XRD patterns of the four types of SiNRs samples. The diffraction peaks are analyzed by XRD software (PCPDFWIN). The standard diffraction lines of cubic silicon and hydroxyapatite are also shown for comparison. (b) FTIR spectra of the SiNRs, exhibiting obvious absorption peaks at 400–4000 cm^{-1}.

with hydroxyapatite (JCPDF card no. 09-0432).[12] Moreover, the broad diffraction peak at 21.5° derived from the highly disordered carbon atoms and amorphous silica, corresponding to surface oxide regions, is slightly observed from all samples (Figure 2a).[13] FTIR spectra of the SiNRs (Figure 2b) show characteristic absorption bands for N–H and O–H stretching vibrations of the amino and hydroxyl groups near 3100 and 3300 cm^{-1}. Two signals at 1010 and 1090 cm^{-1} are for Si–O–Si and Si–O–C vibrations, respectively, confirming the presence of silicon atoms in each sample. The P–O bond of the phosphate group's stretching and bending vibration remained in the same position at 1037 and 604 cm^{-1}.[14] The SiNRs are also characterized by Raman, in which a peak located at 520 cm^{-1} further demonstrates the existence of silicon (Figure S3).

To analyze the chemical compositions of SiNRs with different length, XPS and EDX analyses were performed (Figures S4 and S5), suggesting the presence of Si, C, Ca, P, and O.[15] The high-resolution XPS data support the changes in the compositions of SiNRs. High-resolution XPS of the Si 2p region (Figure 3a–d) shows an intense emission at 99.3 eV characteristic of silicon atoms (i.e., Si(0)); signals arising from Si surface atoms as well as silicon suboxides are observed at

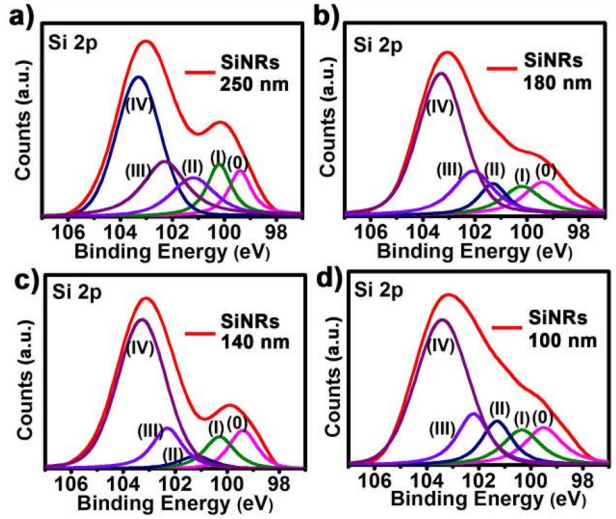

Figure 3. (a–d) Si 2p region of the high-resolution XP spectra of SiNRs with different lengths. Fitting is shown for the Si $2p_{3/2}$ component. The Si $2p_{1/2}$ components have omitted for clarity.

DOI: 10.1021/jacs.6b00479
J. Am. Chem. Soc. 2016, 138, 4824–4831

100.3, 101.3, 102.3, and 103.4 eV.[16] We note that high concentrations of milk yield more intense XP signals associated with silicon suboxides. The contents of silicon in the four types of SiNRs increase in the order of 9% < 11% < 15% < 19% with the enhancement of aspect ratio.

The UV-PL spectra of the four samples, presented in Figure 4a,b, show that the SiNRs possess good optical properties with

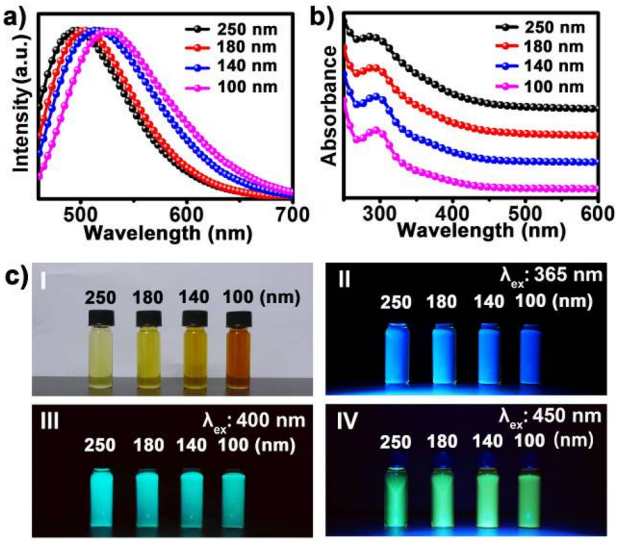

Figure 4. (a) PL ($\lambda_{excitation}$ (λ_{ex}) = 420 nm) spectra and (b) absorption spectra of the SiNRs with different length. (c) Photographs of SiNRs with different lengths under ambient light (I), 365 nm irradiation (II), 400 nm irradiation (II), and 450 nm irradiation (IV).

clearly resolved symmetrical photoluminescence (PL) peaks and absorption peaks. As displayed, the SiNRs show distinguishable PL peaks which progressively shift to longer wavelengths (from 490 to 525 nm) as the nanorods length decreases. In addition, the photoluminescent quantum yield and time-resolved fluorescence decay curves of SiNRs with different lengths are also measured, as shown in Figures S7 and S8. Typically, the fluorescence lifetime spectra of SiNRs (i.e., ~ 7.2 ns of 180 nm SiNRs, Figure S8) are consistent with other time scales (ns) of defect-related emission from silicon nanomaterials with strong blue fluorescence (e.g., silicon nanocrystals), suggesting the strong blue fluorescence of SiNRs is from the exciton recombination at localized defect states, occurring at the surfaces of silicon nanomaterials, similar to the origin of fluorescence of other reported fluorescent silicon materials (e.g., silicon nanoparticles and porous silicon).[17] The position of absorption peaks also follows a similar trend, increasing from ~285 to 305 nm, which corresponds to the nanorods length decreasing from 250 to 100 nm, respectively.

Of particular interest, the as-prepared SiNRs feature excitation wavelength-dependent emission property. Figure 4c displays the four types of SiNRs that emit blue, green, and yellow fluorescence under excitation at 365, 400, and 450 nm, respectively. Corresponding PL spectra are shown in Figure S9, displaying selective emission peaks in a broad color range over the visible region ranging from ~450 to ~600 nm under serial excitation from 390 to 560 nm. In our following experiments, we interrogate the origin of this interesting optical phenomenon in a detailed way. Figure 5 fully records the growth process of one-dimensional SiNRs and presents the corresponding excitation wavelength-dependent emission spectra at different reaction times. Typically, no nanocrystals (Figure 5a) and fluorescence (Figure 5f,k) can be observed at the initial stage (0 min), and then, a number of ultrasmall nanoclusters (~1 nm) appear in the first 10 min of reaction (Figure 5b), corresponding to Step 1 involving micelle fusion and crystal nucleation illustrated in Figure 1a. In this initial stage, the barely visible blue fluorescence has been aroused with excitation wavelength-independent emission (i.e., $\lambda_{emission}$ maintains at ~500 nm) (Figure 5g,l).

In the following 10 min, the small nanoclusters begin to aggregate in a longitudinal direction (Figure 5c). As shown in Figure 5h,m, the samples produce feeble fluorescence, and the excitation wavelength-dependent emission property is observed to some extent, showing in a narrow red-shift range (40 nm) from ~505 to 545 nm under serial excitation from 400 to 510 nm, respectively. Next, the rod-shaped products with relatively inferior dispersity are formed when the reaction is extended to 40 min (Figure 5d), which can display detectable blue, green, and yellow fluorescence under excitation wavelengths of 365, 400, and 450 nm (Figure 5i), respectively, and the red-shift

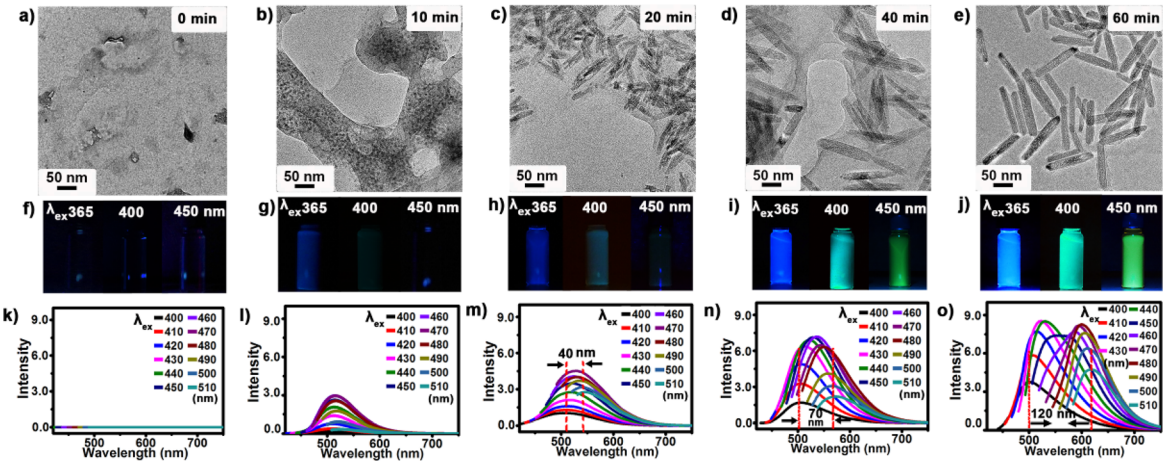

Figure 5. (a–e) TEM images of the SiNRs obtained at different reaction times (0, 10, 20, 40, 60 min) with a milk concentration of 3 mg/mL (reaction temperature: 150 °C). (f–j) Photographs of the SiNRs aqueous solution under 365, 400, and 450 nm irradiation; (k–o) corresponding fluorescence spectra under serial excitation wavelengths from 400 to 510 nm.

DOI: 10.1021/jacs.6b00479
J. Am. Chem. Soc. 2016, 138, 4824–4831

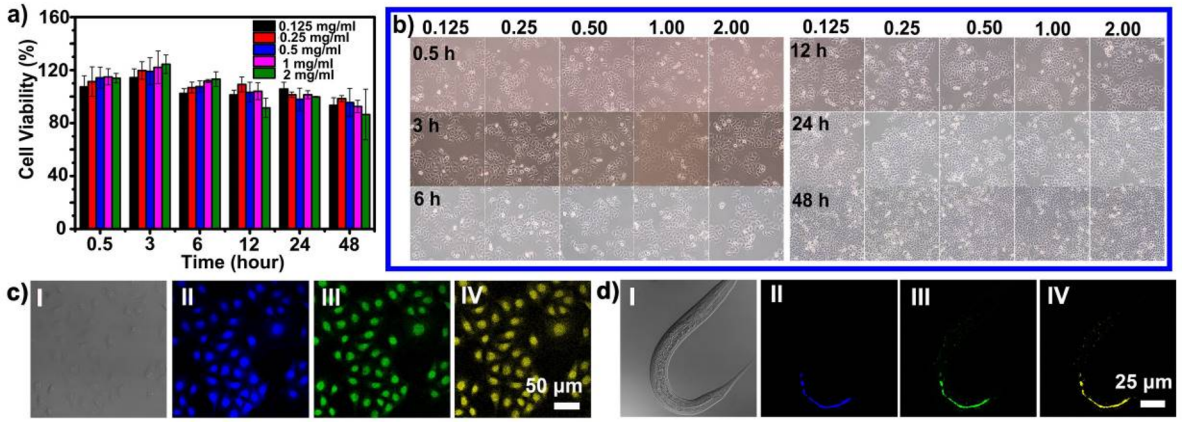

Figure 6. (a) Cell viability of HeLa cells treated with the SiNRs (the SiNRs with length of 140 nm (determined by TEM) are employed as a model) for different incubation times. The viability of the control cells was considered 100%. (b) Morphology of cells incubated with SiNRs of different concentrations (0.125, 0.25, 0.5, 1, 2 mg/mL) for 0.5, 3, 6, 12, 24, and 48 h. Multicolor confocal images of (c) HeLa cells and (d) *C. elegans* treated by the SiNRs. Their corresponding bright-field images are shown in (c (I)) and (d (I)), respectively. The images of (c (II), d (II)) are collected in the ranges of 430−480 nm at λ_{ex} = 405 nm; the images of (c (III), d (III)) are collected in the ranges of 470−550 nm at λ_{ex} = 458 nm; the images of (c (IV), d (IV)) are collected in the ranges of 560−620 nm at λ_{ex} = 514 nm with laser-scanning confocal microscope, respectively.

range of excitation wavelength-dependent emission increases to 70 nm (Figure 5n). The growth process presented in Figure 5c,d is consistent with Step 2 of crystal growth and aggregation, as illustrated in Figure 1a, which has also been reported in other models for the formation of nanomaterials (e.g., TiO_2, ZnO, ZnS, etc.).[18] In the final 20 min of reaction, the distinct excitation wavelength-dependent emission is readily detected (Figure 5j,o) when the SiNRs with ∼140 nm length and good monodispersibility are yielded (Figure 5e). Notably, the broad red-shift range (∼120 nm) over the visible region ranging from ∼500 to ∼620 nm, corresponding to serial excitation from 400 to 510 nm, is observed in the final products of SiNRs (Figure 5o). To further demonstrate such unique optical property of SiNRs, fluorescent carbon nanoparitlces (NPs) and silicon NPs (SiNPs) are used as controls in our experiment. As shown in Figure S1c, while the carbon NPs prepared at the same reaction temperature and time (150 °C/60 min) also exhibit excitation wavelength-dependent emission spectra, the red-shift range only reaches 70 nm (maximum emission wavelength ranges from ∼470 to ∼540 nm under continuous excitation from 400 to 510 nm, respectively, consistent with previously published results),[18d] much narrower than that (∼120 nm) of the SiNRs. Moreover, for the fluorescent SiNPs featuring excitation-independent emission behavior, the maximal emission wavelength maintains ∼495 nm in spite of serial excitation wavelengths ranging 400−510 nm (Figure S1d). These experimental results convincingly demonstrate that the formation of nanorods is responsible for the distinct excitation wavelength-dependent emission property of SiNRs.

In addition to the unique optical properties, the resultant SiNRs exhibit negligible cytotoxicity. Figure 6a exhibits that the cell viability of HeLa cells treated by the SiNRs preserves >90% at different concentrations (0.125−2 mg/mL) and incubation times (0.5−48 h). Figure 6b shows that SiNRs (length: 140 nm)-treated HeLa cells maintain normal morphology during 48 h incubation, indicating undetectable cytotoxicity of the SiNRs. Similarly, cells treated by another three lengths (i.e., 100, 180, and 250 nm) of SiNRs also preserve >90% cellular viability (Figure S10), indicating negligible cytotoxicity of the prepared SiNRs with different lengths. As thus, the observed feeble toxicity and excitation-wavelength-dependent PL endows SiNRs the feasibility in multicolor bioimaging under different excitation wavelengths. In our experiment, the HeLa cells distributed with SiNRs display strong and spectrally resolved fluorescent signals, also exhibiting distinct blue, green and yellow color upon excitation at 405, 458, and 514 nm, respectively (Figure 6c). By utilizing *Caenorhabditis elegans* as an animal model (*C. elegans* is a kind of well-studied nematode with well-defined anatomy),[19] we further testify the possibility of *in vivo* bioimaging using the fluorescent SiNRs. Figure 6d displays overall distribution of the SiNRs in the worm body introduced by feeding, showing intense and spectrally resolved fluorescence. Similar to *in vitro* imaging data, the worm body distributed with the SiNRs also exhibits blue, green, and yellow fluorescence under different excitation wavelength (i.e., blue, green, and yellow fluorescence under 405 nm (Figure 6d (II)), 458 nm (Figure 6d (III)), and 514 nm (Figure 6d (IV)) excitation), suggesting potential application of multicolor imaging *in vitro* and *in vivo*.

Fluorescence stability is of essential importance for practical applications, and we thus further investigate the storage and photostability of the SiNRs in the following experiment. Of particular significance, as shown in Figure 7, the as-prepared SiNRs preserve extremely stable optical properties during long-term storage and high-power UV irradiation. Specifically, the SiNRs maintain high and stable PL intensity during the 100 day storage in ambient environment without any special protection (Figure 7a). We further compare photostability of the as-prepared SiNRs with FITC (one kind of conventional organic dyes) and well-studied II−VI quantum dots (QDs). Figure 7b shows that the fluorescence of FITC quickly quenches in 15 min UV irradiation due to severe photobleaching. While II−VI QDs are more photostable, their fluorescence is nevertheless severely quenched within 45 or 160 min observation for CdTe or CdSe/ZnS, respectively, which is ascribed to long-term UV irradiation-induced surface deterioration. In marked contrast, the SiNRs are strikingly stable, and their fluorescent intensities stay nearly unchanged during 400 min of UV irradiation. Figure 7c−h presents typical photographs of the above samples under UV irradiation for serial irradiation times. For the samples of FITC (Figure 7d), CdTe QDs (Figure 7e), and CdSe/ZnS QDs (Figure 7f), their fluorescence is strong in the beginning

DOI: 10.1021/jacs.6b00479
J. Am. Chem. Soc. 2016, 138, 4824−4831

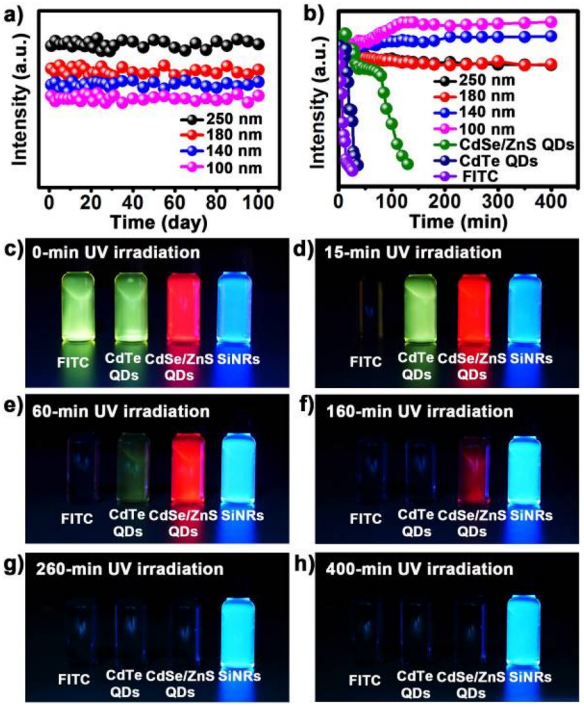

Figure 7. (a) The as-prepared aqueous samples of SiNRs with different length retain nearly identical fluorescent intensity during 100 days of storage. (b) Photostability comparison of aqueous solutions of FITC, CdTe QDs, CdSe/ZnS QDs, and four different aspect ratio SiNRs under continuous UV irradiation (450 W xenon lamp) for serial times. (c–h) Photographs of aqueous solutions of FITC, CdTe QDs, CdSe/ZnS QDs, and SiNRs under continuous UV irradiation (450 W xenon lamp) for serial times.

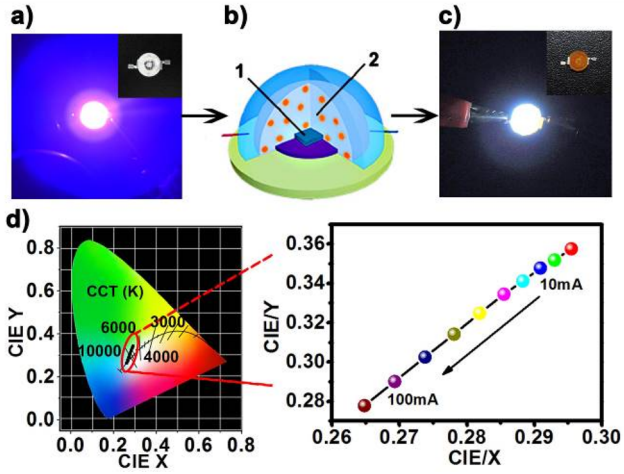

Figure 8. (a) Photographs of the blue LED operated at 5 mA current. (b) Schematic diagram of the SiNRs-based white LED ((1) blue LED chips (emission peak at 420 nm); (2) mixed SiNR-silicone composites). (c) As-prepared SiNRs-based white LED (SiNRs-LED) operated at 10 mA current. (d) The color coordination of the spectrum under various currents (the red circle) on the CIE 1931 color space.

but gradually vanishes as irradiation time increases. Severe fluorescence quench happens within 15, 60, and 160 min of UV irradiation, respectively. In comparison, the SiNRs sample maintains stable and distinct blue fluorescence during 400 min of UV irradiation (Figure 7c–h), additionally demonstrating the ultrahigh photostability of the SiNRs. Similar to photostable zero-dimensional fluorescent silicon nanoparticles, we ascribe such observed high photostability of SiNRs to two possible contributors; these are the protection from stable silica shell and the intrinsic optical properties of silicon nanomaterials.[20]

As proof-of-concept optoelectronic applications, we finally exploit the fluorescent and photostable SiNRs as a novel kind of color converters for constructing the first example of one-dimensional fluorescent silicon nanostructure-based white-emitting LED. Experimentally, the composites of the SiNRs and silicone being deposited on commercially available blue LED chips allow constructing the white LED device, whose illuminating capacity is shown in Figure 8a–c. The LED generates electroluminescence, and its electroluminescence pumps the integrated color conversion layer, which in turn generates white light. During this practice, the partial energy from the LED is absorbed by SiNRs, which is converted to yellow-green light. Typically, the blue LED operated with 5 mA current is shown in Figure 8a. The SiNRs-based LED operated by 10 mA current is presented in Figure 8c, whose color quality is close to an ideal incandescent light source. When excited by a blue LED of 420 nm, the SiNRs emit a broad band yellow-green light. Owing to the mixing of 420 nm and a broad yellow-green emission peaked at 540 nm, the blue light is converted into a white one. Moreover, the resultant SiNRs-based LED device exhibits 12.2 lmW^{-1} efficacy at the coordinate (x, y) = (0.295, 0.357), with a color rendering index (CRI) of 76 and a CCT of 7203K. The external quantum efficiency (EQE) is 42% and 7% for blue and white LED, respectively, which means that a number of blue photons are lost in the SiNRs. Despite the relatively low EQE value, the SiNRs feature a non- or lowly toxic property, simplified fabrication process, and unique optical nature. Such merits make SiNRs a promising candidate for commercial phosphors which often contain expensive sources, such as rare earth.[21a,b] EL spectra of the constructed SiNRs-based LED device under various currents are also investigated. In our devices, the PL bands of SiNRs increase, accompanied by the increase of applied forward current (Figure S11). However, optical properties of the white LED change slightly with the increase of applied forward current. The CIE color coordinates of the SiNR-based white LED vary from (0.295, 0.357) at 10 mA to (0.265, 0.277) at 100 mA, as shown in Figure 8d. This can be explained by aggregation of SiNRs resulting from a new energy band that is formed through overlapping of quantized energy levels.[21]

While these results indicate that SiNRs may act as potential green-yellow tunable phosphors for possible applications in the solid-state lighting industry, there are still some critical issues that need to be addressed. For example, the current 15% QY of SiNRs is not good enough for real LED application when compared with the high QY (>60%) in typical QDs.[22] We therefore acknowledge that intensive investigations should be performed in future work, including but not limited to the improvement of QY values, the optimization of modeling, the simplification of fabrication procedures, and so forth, to obtain a desirable SiNR-based LED device with adaptable EQE, CRI, and color coordinates, which would be suitable for real applications.

CONCLUSION

In summary, we present a kind of biocompatible fluorescent SiNR prepared through a facile one-pot microwave reaction in an aqueous phase. We explore the SiNRs featuring excitation

DOI: 10.1021/jacs.6b00479
J. Am. Chem. Soc. 2016, 138, 4824–4831

wavelength-dependent emission property as biocompatible fluorescent labels for multicolor bioimaging. Taking advantage of the robust photostability and strong fluorescence of the prepared SiNRs, we further demonstrate the feasibility of SiNR-based color converters for the construction of white LED, which is the first example of a LED device, fabricated using the one-dimensional fluorescent silicon nanostructures. Therefore, these results raise exciting opportunities for designing one-dimensional fluorescent silicon nanostructures and facilitate promotion of silicon nanomaterials-based optical applications.

EXPERIMENTAL METHODS

Synthesis of SiNRs. The preparation of precursor solution was based on the addition of (3-aminopropyl) trimethoxysilane of 1 mL to N_2-saturated aqueous solution of 8 mL dispersed with 0.075 g of trisodium citrate. Then, the milk (from 10 to 40 mg) was mixed into the citric acid aqueous solution under constant stirring. The mixture was stirred for 15 min before transferring into the 15 mL exclusive vitreous vessel. The SiNRs were prepared under 150 °C/1 h. After microwave irradiation, the sample was collected when the temperature cooled to lower than 30 °C naturally. The residual reagents such as (3-aminopropyl) trimethoxysilane and trisodium citrate were removed by dialysis (1000 Da). Next, to further purify the as-prepared SiNRs, the obtained solution was centrifuged for 5 min at 8000 rpm (fluorescent carbon nanodots with sizes smaller than ∼5 nm cannot be deposited under this condition),[18d] discarding the supernatant. The precipitate was redispersed in water and centrifuged again at 8000 rpm for 5 min. Such treatment was repeated three times until the supernatant was transparent.[6] Finally, the SiNRs were redispersed in water for further use. In addition, our method is efficacious for synthesis of high-quantity SiNRs, e.g., 0.031 g (250 nm); 0.039 g (180 nm); 0.055 g (140 nm) and 0.076 g (100 nm) SiNRs are readily achieved in a 60 min reaction The purified SiNRs are then used for following characterizations and applications.

Fluorescence Imaging *in Vitro* and *in Vivo*. Fluorescence labeling of fixed HeLa cells used the prepared SiNRs (the SiNRs with length of 140 nm are employed as a model). Human epithelial cervical cancer cells (HeLa cells) were cultured (37 °C, 5% CO_2) on cover glass in Dulbecco's modified Eagle's medium with 10% heat-inactivated fetal bovine serum and antibiotics (100 μg/mL streptomycin and 100 U/ml penicillin) overnight. HeLa cells were fixed with 4% paraformaldehyde for 20 min and blocked for 40 min in PBS containing 4% BSA and 0.1% Triton X-100. Fixed and blocked HeLa cells were incubated sequentially with materials for 12 h. The stained cells were mounted on slides in fluoromount (Sigma, F4680) with coverslips. *C. elegans* wild-type Bristol N2 was provided by the CGC, which was funded by the NIH Office of Research Infrastructure Programs (P40 OD010440). Worms were incubated at 20 °C. L1-arrested worms were fed on an OP50-seeded NGM plate (60 mm) for 24 h then transferred to a fresh plate with 200 μL SiNRs for 12 h. Samples were examined under a confocal laser microscope.

Fabrication of SiNR-Based LED. First, the silicone precursors of Qsil218 and ACC Silicones were mixed at a ratio of 10:1 (v/v). Then, ∼50 μL of silicone precursor mixture was placed on the commercial LED (emission peak at 420 nm, Shenzhen Dongrui Co.). Subsequently, the dried SiNRs were milled to a uniform powder, being spread on the surface of silicone precursor mixture. After the dispersion of the powder within the silicone, the final mixture was cured in air at 60 °C for 2h.

ASSOCIATED CONTENT

Supporting Information

The Supporting Information is available free of charge on the ACS Publications website at DOI: 10.1021/jacs.6b00479.

Additional data (Figures S1−S11) and corresponding discussions (PDF)

AUTHOR INFORMATION

Corresponding Author

*yaohe@suda.edu.cn

Notes

The authors declare no competing financial interest.

ACKNOWLEDGMENTS

We thank Prof. Shuit-Tong Lee's for general help and valuable suggestion. The authors appreciate financial support from the National Basic Research Program of China (973 Program 2013CB934400, 2012CB932400), NSFC (61361160412, 31400860), and Projects Funded by the Priority Academic Program Development of Jiangsu Higher Education Institutions (PAPD), and China Postdoctoral Science Foundation (7131701914), as well as Collaborative Innovation Center of Suzhou Nano Science and Technology (NANO-CIC).

REFERENCES

(1) (a) Dasgupta, N. P.; Liu, C.; Andrews, S.; Prinz, F. B.; Yang, P. D. *J. Am. Chem. Soc.* **2013**, *135*, 12932−12935. (b) Xie, P.; Xiong, Q. H.; Fang, Y.; Qing, Q.; Lieber, C. M. *Nat. Nanotechnol.* **2012**, *7*, 119−125. (c) Wu, H.; Chan, G.; Choi, J. W.; Ryu, I.; Yao, Y.; McDowell, M. T.; Lee, S. W.; Jackson, A.; Yang, Y.; Hu, L. B.; Cui, Y. *Nat. Nanotechnol.* **2012**, *7*, 310−315. (d) Howes, P. D.; Chandrawti, R.; Stevens, M. M. *Science* **2014**, *346*, 1247390. (e) Cheng, X. Y.; Lowe, S. B.; Reece, P. J.; Gooding, J. J. *Chem. Soc. Rev.* **2014**, *43*, 2680−2700. (f) McVey, B. F. P.; Tilley, R. D. *Acc. Chem. Res.* **2014**, *47*, 3045−3051. (g) Dasog, M.; Kehrle, J.; Rieger, B.; Veinot, J. G. C. *Angew. Chem., Int. Ed.* **2016**, *55*, 2322−2339. (h) Chiappini, C.; Rosa, D. E.; Martinez, J. O.; Liu, X.; Steele, J.; Stevens, M. M.; Tasciotti, E. *Nat. Mater.* **2015**, *14*, 532−539. (i) Qian, C.; Sun, W.; Wang, L.; Chen, C.; Liao, K.; Wang, W.; Jia, J.; Hatton, B. D.; Casillas, G.; Kurylowicz, M.; Yip, C. M.; Mastronardi, M. L.; Ozin, G. A. *J. Am. Chem. Soc.* **2014**, *136*, 15849−15852.

(2) (a) Patolsky, F.; Timko, B. P.; Yu, G. H.; Fang, Y.; Greytak, A. B.; Zheng, G. F.; Lieber, C. M. *Science* **2006**, *313*, 1100−1104. (b) Qing, Q.; Jiang, Z.; Xu, L.; Gao, R. X.; Mai, L. Q.; Lieber, C. M. *Nat. Nanotechnol.* **2014**, *9*, 142−147. (c) Resasco, J.; Dasgupta, N. P.; Rosell, J. R.; Guo, J. H.; Yang, P. D. *J. Am. Chem. Soc.* **2014**, *136*, 10521−10526. (d) Duan, X. F.; Huang, Y.; Agarwal, R.; Lieber, C. M. *Nature* **2003**, *421*, 241−245. (e) Hochbaum, A. I.; Yang, P. D. *Chem. Rev.* **2010**, *110*, 527−546. (f) Cui, Y.; Wei, Q.; Park, H.; Lieber, C. M. *Science* **2001**, *293*, 1289−1292. (g) Li, B. R.; Hsieh, Y. J.; Chen, Y. X.; Chung, Y. T.; Pan, C. Y.; Chen, Y. T. *J. Am. Chem. Soc.* **2013**, *135*, 16034−16037. (h) Gao, C. B.; Zhang, Q.; Lu, Z. D.; Yin, Y. D. *J. Am. Chem. Soc.* **2011**, *133*, 19706−19709.

(3) (a) Liu, J.; Fu, T. M.; Cheng, Z. G.; Hong, G. S.; Zhou, T.; Jin, L. H.; Duvvuri, M.; Jiang, Z.; Kruskal, P.; Xie, C.; Suo, Z. G.; Fang, Y.; Lieber, C. M. *Nat. Nanotechnol.* **2015**, *115*, 629−636. (b) Tian, B.; Liu, J.; Dvir, T.; Jin, L.; Tsui, J. H.; Qing, Q.; Suo, Z.; Langer, R.; Kohane, D. S.; Lieber, C. M. *Nat. Mater.* **2012**, *11*, 986−994.

(4) (a) Garnett, E. C.; Yang, P. D. *J. Am. Chem. Soc.* **2008**, *130*, 9224−9225. (b) Liu, C.; Gallagher, J. J.; Sakimoto, K. K.; Nichols, E. M.; Chang, C. J.; Chang, M. C. Y.; Yang, P. D. *Nano Lett.* **2015**, *15*, 3634−3639. (c) Kim, W.; Ng, J. K.; Kunitake, M. E.; Conklin, B. R.; Yang, P. D. *J. Am. Chem. Soc.* **2007**, *129*, 7228−7229. (d) Priolo, F.; Gregorkiewicz, T.; Galli, M.; Krauss, T. F. *Nat. Nanotechnol.* **2014**, *9*, 19−32. (e) Chockla, A. M.; Harris, J. T.; Akhavan, V. A.; Bogart, T. D.; Holmberg, V. C.; Steinhagen, C.; Mullins, C. B.; Stevenson, K. J.; Korgel, B. A. *J. Am. Chem. Soc.* **2011**, *133*, 20914−20921. (f) Miao, R.; Mu, L. X.; Zhang, H. Y.; She, G. W.; Zhou, B. J.; Xu, H. T.; Wang, P. F.; Shi, W. S. *Nano Lett.* **2014**, *14*, 3124−3129. (g) Xie, Z.; Henderson, E. J.; Dag, O.; Wang, W.; Lofgreen, J. E.; Kübel, C.; Scherer, T.; Brodersen, P. M.; Gu, Z. Z.; Ozin, G. A. *J. Am. Chem. Soc.* **2011**, *133*, 5094−5102. (h) Liu, X. H.; Fan, F.; Yang, H.; Zhang, S.; Huang, J. Y.; Zhu, T. *ACS Nano* **2013**, *7*, 1495−1503. (i) Peng, F.; Su, Y. Y.; Wei, X. P.; Lu, Y. M.; Zhou, Y. F.; Zhong, Y. L.; Lee, S. T.; He, Y. *Angew. Chem., Int. Ed.* **2013**, *52*, 1457−1461.

DOI: 10.1021/jacs.6b00479
J. Am. Chem. Soc. 2016, 138, 4824−4831

(5) (a) Zheng, J. Y.; Yan, Y. L.; Wang, X. P.; Zhao, Y. S.; Huang, J. X.; Yao, J. N. *J. Am. Chem. Soc.* **2012**, *134*, 2880−2883. (b) Wu, K. F.; Du, Y. L.; Tang, H.; Chen, Z. Y.; Lian, T. Q. *J. Am. Chem. Soc.* **2015**, *137*, 10224−10230. (c) Shabaev, A.; Hellberg, C. S.; Efros, A. L. *Acc. Chem. Res.* **2013**, *46*, 1242−1251. (d) Brus, L.; Szajowski, P.; Wilson, W.; Harris, T.; Schuppler, S.; Citrin, P. *J. Am. Chem. Soc.* **1995**, *117*, 2915−2922. (e) Wilson, W. L.; Szajowski, P.; Brus, L. *Science* **1993**, *262*, 1242−1244. (f) Wang, Q. Q.; Xu, B.; Sun, J.; Liu, H. Y.; Zhao, Z. S.; Yu, D. L.; Fan, C. Z.; He, J. L. *J. Am. Chem. Soc.* **2014**, *136*, 9826−9829.

(6) (a) Heitsch, A. T.; Fanfair, D. D.; Tuan, H. Y.; Korgel, B. A. *J. Am. Chem. Soc.* **2008**, *130*, 5436−5437. (b) Heitsch, A. T.; Hessel, C. M.; Akhavan, V. A.; Korgel, B. A. *Nano Lett.* **2009**, *9*, 3042−3047. (c) Lu, X. T.; Hessel, C. M.; Yu, Y. X.; Bogart, T. D.; Korgel, B. A. *Nano Lett.* **2013**, *13*, 3101−3105.

(7) (a) Peng, F.; Su, Y. Y.; Zhong, Y. L.; Fan, C. H.; Lee, S. T.; He, Y. *Acc. Chem. Res.* **2014**, *47*, 612−623. (b) He, Y.; Zhong, Y. L.; Peng, F.; Wei, X. P.; Su, Y. Y.; Lu, Y. M.; Su, S.; Gu, W.; Liao, L. S.; Lee, S. T. *J. Am. Chem. Soc.* **2011**, *133*, 14192−14195. (c) Zhong, Y. L.; Peng, F.; Bao, F.; Wang, S. Y.; Ji, X. Y.; Yang, L.; Su, Y. Y.; Lee, S. T.; He, Y. *J. Am. Chem. Soc.* **2013**, *135*, 8350−8356. (d) Wu, S. C.; Zhong, Y. L.; Zhou, Y. F.; Song, B.; Chu, B. B.; Ji, X. Y.; Wu, Y. Y.; Su, Y. Y.; He, Y. *J. Am. Chem. Soc.* **2015**, *137*, 14726−14732. (e) He, Y.; Kang, Z. H.; Li, Q. S.; Tsang, C. H. A.; Fan, C. H.; Lee, S. T. *Angew. Chem., Int. Ed.* **2009**, *48*, 128−132. (f) He, Y.; Su, Y. Y.; Yang, X. B.; Kang, Z. H.; Xu, T. T.; Zhang, R. Q.; Fan, C. H.; Lee, S. T. *J. Am. Chem. Soc.* **2009**, *131*, 4434−4438.

(8) (a) Wiedman, G.; Fuselier, T.; He, J.; Searson, P. C.; Hristova, K.; Wimley, W. C. *J. Am. Chem. Soc.* **2014**, *136*, 4724−4731. (b) López-Pelegrín, M.; Cerdà-Costa, N.; Cintas-Pedrola, A.; Herranz-Trillo, F.; Bernadó, P.; Peinado, J. R.; Arolas, J. L.; Gomis-Rüth, F. X. *Angew. Chem., Int. Ed.* **2014**, *53*, 10624−10630.

(9) (a) Sadat-Shojai, M.; Khorasani, M. T.; Ehsan, D. K.; Ahmad, J. *Acta Biomater.* **2013**, *9*, 7591−7621. (b) Richman, M.; Wilk, S.; Chemerovski, M.; Wärmländer, S. K.; Wahlström, A.; Gräslund, A.; Rahimipour, S. *J. Am. Chem. Soc.* **2013**, *135*, 3474−3484. (c) Mostaghaci, B.; Loretz, B.; Haberkorn, R.; Kickelbick, G.; Lehr, C. M. *Chem. Mater.* **2013**, *25*, 3667−3674.

(10) (a) Sun, S.; Zeng, H. *J. Am. Chem. Soc.* **2002**, *124*, 8204−8205. (b) Watzky, M. A.; Finke, R. G. *J. Am. Chem. Soc.* **1997**, *119*, 10382−10400. (c) LaMer, V. K.; Dinegar, R. H. *J. Am. Chem. Soc.* **1950**, *72*, 4847−4854.

(11) (a) Purkait, T. K.; Iqbal, M.; Wahl, M. H.; Gottschling, K.; Gonzalez, C. M.; Islam, M. A.; Veinot, J. G. C. *J. Am. Chem. Soc.* **2014**, *136*, 17914−17917. (b) Dasog, M.; Yang, Z. Y.; Regli, S.; Atkins, T. M.; Faramus, A.; Singh, M. P.; Muthuswamy, E.; Kauzlarich, S. M.; Tilley, R. D.; Veinot, J. G. C. *ACS Nano* **2013**, *7*, 2676−2685.

(12) (a) Cullis, A. G.; Canham, L. T. *Nature* **1991**, *353*, 335−338. (b) Ma, J.; Qin, J. L. *Cryst. Growth Des.* **2015**, *15*, 1273−1279.

(13) Qu, S. N.; Wang, X. Y.; Lu, Q. P.; Liu, X. Y.; Wang, L. J. *Angew. Chem., Int. Ed.* **2012**, *51*, 12215−12218.

(14) (a) Chen, C. L.; Rosi, N. L. *Angew. Chem., Int. Ed.* **2010**, *49*, 1924−1942. (b) Mi, P.; Dewi, N.; Yanagie, H.; Kokuryo, D.; Suzuki, M.; Sakurai, Y.; Li, Y.; Aoki, I.; Ono, K.; Takahashi, H.; Cabral, H.; Nishiyama, N.; Kataoka, K. *ACS Nano* **2015**, *9*, 5913−5921.

(15) (a) Weidner, T.; Dubey, M.; Breen, N. F.; Ash, J.; Baio, J. E.; Jaye, C.; Fischer, D. A.; Drobny, G. P.; Castner, D. G. *J. Am. Chem. Soc.* **2012**, *134*, 8750−8753. (b) Rim, H. P.; Min, K. H.; Lee, H. J.; Jeong, S. Y.; Lee, S. C. *Angew. Chem., Int. Ed.* **2011**, *50*, 8853−8857.

(16) (a) Yang, Z. Y.; Iqbal, M.; Dobbie, A. R.; Veinot, J. G. C. *J. Am. Chem. Soc.* **2013**, *135*, 17595−17601. (b) Purkait, T. K.; Iqbal, M.; Wahl, M. H.; Gottschling, K.; Gonzalez, C. M.; Islam, M. A.; Veinot, J. G. C. *J. Am. Chem. Soc.* **2014**, *136*, 17914−17917.

(17) (a) Godefroo, S.; Hayne, M.; Jivanescu, M.; Stesmans, A.; Zacharias, M.; Lebedev, O. I.; Van Tendeloo, G.; Moshchalkov, V. V. *Nat. Nanotechnol.* **2008**, *3*, 174−178. (b) Wilcoxon, J. P.; Samara, G. A.; Provencio, P. N. *Phys. Rev. B: Condens. Matter Mater. Phys.* **1999**, *60*, 2704. (c) Hessel, C. M.; Henderson, E. J.; Kelly, J. A.; Cavell, R. G.; Sham, T. K.; Veinot, J. G. C. *J. Phys. Chem. C* **2008**, *112*, 14247−14254.

(18) (a) Penn, R. L.; Banfield, J. F. *Science* **1998**, *281*, 969−971. (b) Yu, J. H.; Joo, J.; Park, H. M.; Baik, S. I.; Kim, Y. W.; Kim, S. C. *J. Am. Chem. Soc.* **2005**, *127*, 5662−5670. (c) Pacholski, C.; Kornowski, A.; Weller, H. *Angew. Chem., Int. Ed.* **2002**, *41*, 1188−1191. (d) Wang, J.; Peng, F.; Lu, Y. M.; Zhong, Y. L.; Wang, S. Y.; Xu, M. F.; Ji, X. Y.; Su, Y. Y.; Liao, L. S.; He, Y. *Adv. Opt. Mater.* **2015**, *3*, 103−111.

(19) Ma, P. A.; Xiao, H. H.; Li, X. X.; Li, C. X.; Dai, Y. L.; Cheng, Z. Y.; Jing, X. B.; Lin, J. *Adv. Mater.* **2013**, *25*, 4898−4905.

(20) (a) He, Y.; Zhong, Y. L.; Su, Y. Y.; Lu, Y. M.; Jiang, Z. Y.; Peng, F.; Xu, T. T.; Su, S.; Huang, Q.; Fan, C. H.; Lee, S. T. *Angew. Chem., Int. Ed.* **2011**, *50*, 5695−5698. (b) Godefroo, S.; Hayne, M.; Jivanescu, M.; Stesmans, A.; Zacharias, M.; Lebedev, O. I.; Tendeloo, G.; Moshchalkov, V. V. *Nat. Nanotechnol.* **2008**, *3*, 174−178.

(21) (a) Ghosh, B.; Masuda, Y.; Wakayama, Y.; Imanaka, Y.; Inoue, J.; Hashi, K.; Deguchi, K.; Yamada, H.; Sakka, Y.; Ohki, S.; Shimizu, T.; Shirahata, N. *Adv. Funct. Mater.* **2014**, *24*, 7151−7160. (b) Erdem, T.; Demir, H. V. *Nat. Photonics* **2011**, *5*, 126−126. (c) Park, W. B.; Singh, S. P.; Sohn, K. S. *J. Am. Chem. Soc.* **2014**, *136*, 2363−2373. (d) Tsai, Y. T.; Chiang, C. Y.; Zhou, W. Z.; Lee, J. F.; Sheu, H. S.; Liu, R. S. *J. Am. Chem. Soc.* **2015**, *137*, 8936−8939.

(22) (a) Jang, E.; Jun, S.; Jang, H.; Lim, J.; Kim, B.; Kim, Y. *Adv. Mater.* **2010**, *22*, 3076−3080. (b) Hou, L.; Zhang, Q.; Ling, L.; Li, C. X.; Chen, L.; Chen, S. *J. Am. Chem. Soc.* **2013**, *135*, 10618−10621.

DOI: 10.1021/jacs.6b00479
J. Am. Chem. Soc. 2016, 138, 4824−4831